Available online at www.sciencedirect.com

ScienceDirect

Procedia Engineering 10 (2011) 3429–3434

Engineering Procedia

ICM11

# Experimental and numerical characterization of anisotropic damage evolution of forged Al6061-T6 alloy

Y. Shen[a]*, J. Garnier[a], L. Allais[a], J. Crepin[b], O. Ancelet[c], J.-M. Hiver[d]

[a]*CEA/DEN/DANS/DMN/SRMA, 91191 Gir-sur-yvette, France*
[b]*ENSMP, Centre des Matériaux, UMR CNRS 7633 91003 Evry, France*
[c]*CEA/DEN/DM2S/SEMT 91191 Gif-sur-vette, France*
[d]*Laboratoire de Physique des Matériaux, UMR CNRS 7556, Ecole des Mines de Nancy, Parc de Saurupt 54042 Nancy, France*

**Abstract**

Aluminum alloy 6061-T6 (Al-Mg-Si) has been selected as the material of the vessel for the construction of Jules-Horowitz material testing reactor. Fracture mechanism of this alloy has been investigated using mechanical testing of smooth and notched tensile specimens loaded in different directions. A strong anisotropic fracture behavior has been observed. Microstructural studies using tomography and image analysis have shown a presence of anisotropic distributed coarse precipitates which is the key microstructural feature affecting the damage evolution. These observations were complemented by investigations on fractured tensile samples. A damage scenario of anisotropic growth and coalescence of voids is proposed to explain the fracture behavior associated with the distribution of precipitates. A GTN (Gurson-Tvergaard-Needleman) damage model is used to simulate this scenario and to predict damage evolution.



*Keywords: Damage; Aluminium alloy 6061-T6; Anisotropy; Microstructural; Modelling*

## 1. Introduction

The aluminum alloy 6061-T6 was selected as the material of the vessel for the Jules-Horowitz material testing reactor for its high neutron transparency, good corrosion resistance, and good mechanical

* Corresponding author. Tel.: +33-169085665; fax: +33-169087167.
*E-mail address*: yang.shen@cea.fr.

properties on operational temperature. Since the vessel of this reactor is irradiated and pressurized, a good compromise between strength and damage tolerance is required [1].

From literatures, it is clear that damage initiates preferentially on coarse precipitates which form voids by particle fracture or interface decohesion [2]. The ductile fracture is then induced by growth and coalescence of these voids [3]. In this paper, we focus on the experimental and numerical characterization of influence of coarse precipitates on the anisotropic damage evolution for the aluminum alloy 6061-T6.

## 2. Material and methods

The material used in this study is a forged vessel of Al6061, as received in a T6 condition (homogenization heat treated, hot forged, solution heat treated, water quenched and ageing).The chemical composition of the alloy is given in Table 1.

Table 1 Chemical composition of Al6061 alloy

| Element | Si | Mg | Fe | Cr | Cu | Mn | Zn | Ti |
|---|---|---|---|---|---|---|---|---|
| Wt.% | 0,65 | 1,01 | 0,24 | 0,18 | 0,30 | 0,09 | 0,20 | 0,02 |

The anisotropy of damage was determined by tensile tests along principal directions: A (axial), R (Radius), C (circumferential) on room temperature. Smooth round specimens were machined with a diameter of 4 mm. The cross-head speed was adjusted so that the strain rate was about to 5 $10^{-4}$ $s^{-1}$. Fracture surfaces were observed by Scanning Electron Microscope (SEM) and the roughness of these surfaces was measured by scanning focus variation microscope [4].

Coarse precipitates were quantitatively characterized by means of image analysis from metallographic observations of SEM. Metallographic observations were also carried out after the chemical treatment of anodic oxidation to reveal grains. These observations by Optical Microscope (OM) were used in the three observation planes: R-C, A-C and A-R in order to analyze the anisotropic features. Tridimensional observations were performed by the X-ray tomography with a resolution of 1,5 $\mu m^3$. Gallium liquid was penetrated in the aluminum to reveal the grain boundaries so that the real grain form can be characterized.

Notched round specimens with a maximum diameter of 10 mm were machined with notch radii of 2 mm, 4 mm and 10 mm (AE2, AE4, AE10) respectively, in order to impose different levels of stress triaxiality during tensile tests. For each test, two laser micrometers scanned the specimen so that diameter reduction and the real-time notch form could be measured.

Finite element computations were performed on these notched specimens employing the GTN damage model [5-7]. The model was implemented in the finite element software *Cast3m*. The flow properties of material used in the simulation were determined by the tensile tests of smooth round specimens with the same maximum diameter after the Bridgman correction [8]. It is observed by in-situ tensile tests that immediate debonding between the matrix and the coarse precipitates $Mg_2Si$ takes place [9]. As a result, the initial porosity $f_0$ used in the GTN model is estimated as the volume fraction of precipitates $f_p$ which is measured by image analysis [10]. Porosity at final failure $f_f$ was adjusted by the comparison of experimental and numerical curves. At the first stage of the study, we suppose that the critical porosity of void coalescence $f_c$ is equal to the volume fraction of voids at final failure $f_f$. Due to symmetry of the sample modeling is done using 2D axisymmetric conditions. Two-dimensional 8-node elements with 9 integration points are used for this simulation. The loading is realized by a prescribed displacement at the top edge.

## 3. Results and discussions

### 3.1. Microstructure

Microstructure has been observed by SEM after the electrochemical treatment. The coarse precipitates are distributed along the grain boundaries as shown in Fig. 1a. An elongation of grains is observed in the plane A-R and the plane A-C along the axial direction as presented in Fig. 1b so that precipitates are aligned through this direction. Fig. 1c shows some isolated grains observed by X-ray tomography after gallium metal liquid penetration [11]. This observation confirms the elongated shape of grains for this material. The average tridimensional grain size is estimated to 70µm*140µm*700µm.

A two-dimensional quantitative study of coarse precipitates is carried out by image analysis in the three observation planes (Table 2). No significant anisotropy of the area fraction, the density or the average size of precipitates is observed in the three planes. In fact, this conclusion has been verified by Hillard and Delesse that the area fraction is equal to the volume fraction statistically [12, 13].

Table 2 Quantification of coarse precipitates: $Mg_2Si$ and iron rich intermetallics (IM_Fe)

| Observation plane | R-C | | A-C | | A-R | | Average | |
|---|---|---|---|---|---|---|---|---|
| Precipitates | $Mg_2Si$ | IM_Fe | $Mg_2Si$ | IM_Fe | $Mg_2Si$ | IM_Fe | $Mg_2Si$ | IM_Fe |
| Area fraction, $f_p$ (%) | 0,9 | 0,7 | 1,0 | 0,5 | 0,9 | 0,7 | 0,9 | 0,6 |
| Density, $d_p$ ($10^{-4}$/µm²) | 8,9 | 39,4 | 8,0 | 22,8 | 7,9 | 36,4 | 8,3 | 32,9 |
| Average size (µm²) | 10,1 | 1,6 | 12,2 | 2,2 | 10,8 | 1,8 | 11,0 | 1,9 |

During the morphological characterization of microstructure of the alloy, we are mainly interested in the coarse precipitates ($Mg_2Si$ and iron rich intermetallics). This shows that the microstructural anisotropy is essentially an anisotropic distribution of these precipitates. Some authors mentioned that the key microstructural feature affecting the void nucleation and growth in Al6061 is the presence of coarse iron rich intermetallics [2, 3]. However, with the presence of abundant brittle $Mg_2Si$, the effect of these intermetallics is of minor importance in our case [9, 14].

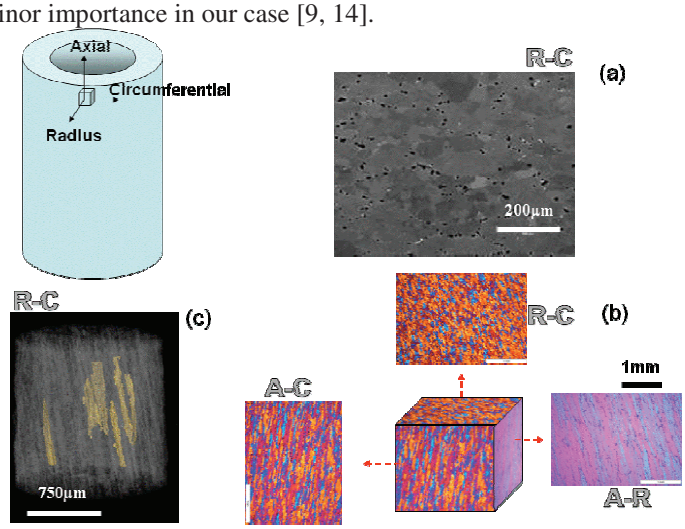


Fig. 1. Microstructure of the Al6061-T6 taken from the vessel: (a) observations of coarse precipitates by SEM (precipitates $Mg_2Si$ on black and iron rich intermetallic particles on white); (b) observations of grains by OM after chemical treatment of anodic oxidation; (c) observation of grains by X-ray tomography with gallium liquid penetrated in grain boundaries

### 3.2. Mechanical tests

#### 3.2.1. Smooth specimens

Table 3 summarizes the mechanical properties of the Al6061-T6 alloy determined from tensile tests for three loading directions. A slight anisotropy on values of yield stress (YS) and ultimate tensile strength (UTS) is measured, while the anisotropy of the fracture strain is marked. The maximum of ductility is found for the A loading direction and the minimum is for the C direction. It turns out that the reduction of area (RA) measured after fracture varies linearly with the fracture strain confirming that the anisotropy of fracture strain measured in tensile tests is mainly induced by anisotropy of damage.

Table 3 Tensile properties for smooth specimens

| Loading Orientation | 0,2% YS (MPa) | UTS (MPa) | Strain at UTS (%) | Fracture strain (%) | RA (%) |
|---|---|---|---|---|---|
| A | 287 | 330 | 7,9 | 15,8 | 42,4 |
| R | 308 | 340 | 6,4 | 11,5 | 29,2 |
| C | 314 | 348 | 5,4 | 9,2 | 22,8 |

#### 3.2.2. Fractography

Fracture surfaces of these smooth tensile specimens are examined by means of SEM and the roughness of these surfaces is measured to compare the anisotropy of damage quantitatively. Fig. 2 shows the fracture surfaces for both loading directions A and C. A large number of dimples with a size about 10-30 µm are observed which indicates the ductile fracture's type. It is observed from area analyses that the roughness of the fracture surface for the A loading direction is stronger than for the C direction. Three profile analyses are carried out through three paths. Some valleys with characteristic longer of about 260µm are observed in Fig. 2e for the path 1 with a depth $Z_A$ of about 150µm. This characteristic longer is related to the grain head size. We observe, for the C loading specimen, a characteristic direction linked with the elongation direction of grains. Profile analysis parallel to this direction is showed in Fig. 2f (path 2) with $Z_{C\text{-parallel}}$ around 50µm and a characteristic longer of 800µm while the analysis perpendicular to this direction in Fig. 2g (path 3) shows a $Z_{C\text{-perpendicular}}$ around 100µm with a longer of about 400µm. These characteristic dimensions are related to the grain size on elongation and transverse directions.

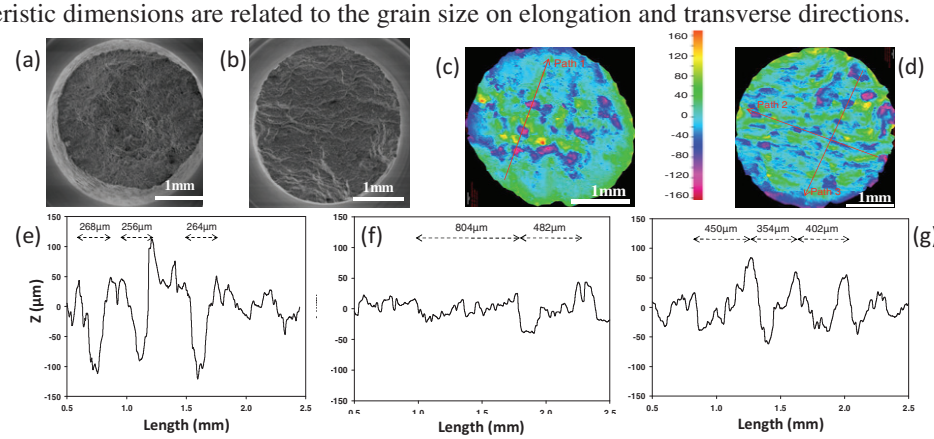


Fig. 2 Fracture surfaces of smooth bars for (a) axial loading direction and (b) circumferential loading direction and the analyses of roughness for surfaces perpendicular to the (c) A direction and (d) C direction; profile roughness measurements (e), (f) and (g) correspond to path 1, path 2 and path 3 respectively.

### 3.3. Ductile fracture simulation

A scenario of damage including the anisotropic distribution of coarse precipitates seems to explain the anisotropy of damage evolution. The fracture occurs when there is percolation of a continuous path of cavities in a plane perpendicular to the loading direction. Voids in these planes have a large growth rate so neighboring precipitates (circled in red in the Fig. 3) form planes of cavities that are perpendicular to the loading direction. The fracture depends then largely on the coalescence rate among the planes of voids parallel to the loading direction. Fig. 3 illustrates precipitates distributed on grains boundaries in both A and C loading directions, where H denotes the average distance between planes of voids perpendicular to the tensile direction. In the case of a tensile test in A direction (Fig. 3a), the fracture is rather difficult because $H_A$ is relatively large: the stage of coalescence requires a significant growth of voids. In the case of a tensile test in C loading direction (Fig. 3b), the coalescence of voids between these planes is easier because $H_C$ is small. As a result, the fracture is easier in the C loading direction than in the A loading direction, which is entirely consistent with the measured values of tensile ductility. The dimple or relief depth in the fracture surfaces confirms this scenario with $Z_A > Z_C$ corresponding part of the distance H.

This scenario can be simulated on notched round bars employing GTN damage model. Table 4 shows parameters used in this model and the experimental fracture strain ($\varepsilon_f$) obtained experimentally. The growth of cavities is supposed to be isotropic. Fig. 4a and b show the tensile force and mean void volume fraction on the most damaged region versus diameter reduction. It is concluded that GTN model can better simulate the material tensile properties than simulations without damage model. With the same initial porosity, loading in C direction presents a bigger gap between experimental results and simulations than loading in A direction for AE4 and AE2 which means that the material degrades earlier and stronger in the C loading direction. The anisotropic feature is contained in porosity at final failure $f_f$. This value is larger in A loading direction than C loading direction. The higher the notch radii, the larger the difference of porosity at failure between the two loading directions is marked.

## 4. Conclusions

These investigations provide experimental and numerical characterizations of damage evolution for the forged Al6061-T6 alloy which is chosen to be the vessel material for the construction of European testing reactor. The anisotropic damage evolution is principally due to the anisotropic distribution of coarse intergranular precipitates. The GTN constitutive damage model can be used to simulate the flow properties and the damage behavior causing by coarse precipitates. However, the identification of parameters in the model can't be deduced by the simple geometrical relationship. Multiphase simulations including voids on grain boundaries and several grains are planned to account for the voids coalescence procedure so as to identify parameters for anisotropic GTN model, especially the porosity on final failure values.

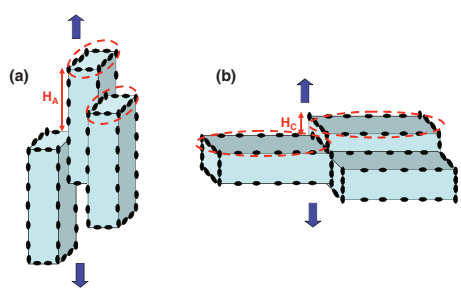


Fig. 3 Two scenarii of damage including the distribution of coarse precipitates: (a) axial direction; (b) circumferential direction

Table 4 Simulation results and model parameters used in the simulations of fracture of notched round specimens

| Notch radii (mm) | AE2 | | AE4 | | AE10 | |
|---|---|---|---|---|---|---|
| Loading direction | A | C | A | C | A | C |
| $f_0$ (%) | 0.9 | 0.9 | 0.9 | 0.9 | 0.9 | 0.9 |
| $f_f$ (%) | 1.25 | 1.1 | 1.55 | 1.1 | 2 | 1.21 |
| $\varepsilon_f$ (%) | 7.65 | 4.46 | 10.38 | 4.44 | 20.89 | 7.90 |

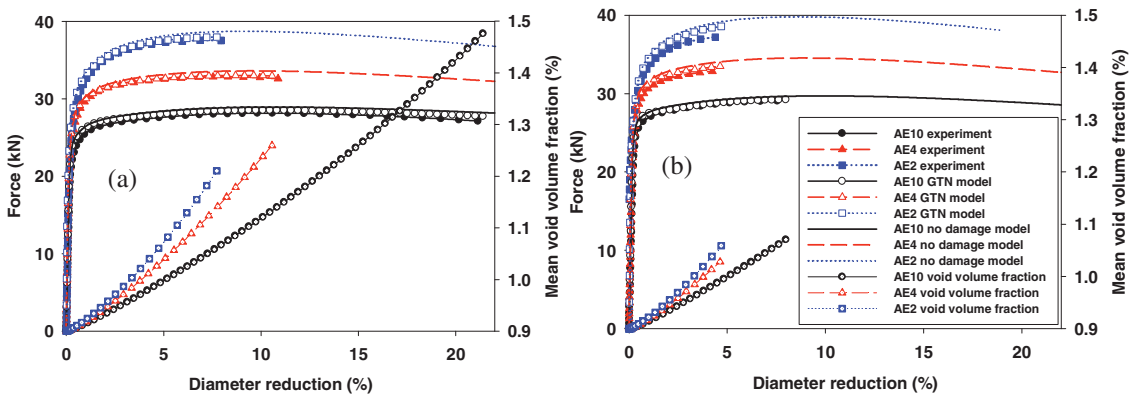


Fig. 4 Results of the tensile tests and the simulations for axial loading direction: force (kN) and mean void volume fraction on the most damaged region (%) vs diameter reduction (%) curves: (a) axial loading direction; (b) circumferential loading direction

## References

[1] G. S. Ning, Y. C. XU, Z. F. Tong, C. Y. Zhang, H. Lin, W. Yang, Atomic Energy Science and Technology 41, Suppl. (2007) 327-360.

[2] D. Lassance, D. Fabregue, F. Delannay, T. Pardoen, Prog. Mat. Sci. 52 (2007) 62-129.

[3] H. Agarwal, A. M. Gokhale, S. Graham, M. F. Horstemeyer, Materials Science and Engineering A 341 (2003) 35-42.

[4] T. Ficker, D. Martisek, H. M. Jennings, Cement and Concrete Research 40 (2010) 947.

[5] V. Tvergaard, Int. J. Fract. 17 (1981) 389-407.

[6] A. L. Gurson, Journal of engineering mateirals technology 99 (1977) 2-15.

[7] A. Needleman, V. Tvergaard, J. Mech. Phys. Solids 32 (1984) 461-490.

[8] P. W. Bridgman, Studies in large plastic flow and fracture with special emphasis on the effects of hydrostatic pressure, McGraw-Hill, New York, 1952, p. x, 362 p.

[9] Y. Shen, J. Garnier, L. Allais, J. Crépin, D. Caldemaison, E. Héripré, J.-M. Hiver, P. Forget, Matériaux 2010 (2010).

[10] T. Pardoen, Computers & Structures 84 (2006) 1641.

[11] T. F. Morgeneyer, M. J. Starink, S. C. Wang, I. Sinclair, Acta Mater. 56 (2008) 2872-2884.

[12] J. E. Hillard (Ed.) Quantitative microscopy, part 3: Measurement of volume in volume, McGraw-Hill Book Company, 1968, p.

[13] A. Delesse (Ed.) Procédé mécanique: pour déterminer la composition des roches, 1848, p. 379-388.

[14] Y. Lee, Y. Kwon, J. Lee, C. Park, S. Kimb, Mat. Sci. \& Eng. A362 (2003) 187-191.